PROCEEDINGS, Thirty-Eighth Workshop on Geothermal Reservoir Engineering
Stanford University, Stanford, California, February 11-13, 2013
SGP-TR-198

3D inversion of magnetotelluric (MT) resistivity data from Krýsuvík high temperature geothermal area in SW Iceland

Gylfi Páll Hersir, Knútur Árnason and Arnar Már Vilhjálmsson

Iceland GeoSurvey (ÍSOR)
Grensásvegur 9, 108 Reykjavík, Iceland
e-mail: gph@isor.is

ABSTRACT

A 3D inversion was performed of static shift corrected off-diagonal impedance tensor elements of 102 MagnetoTelluric (MT) resistivity soundings from the Greater Krýsuvík geothermal area, SW Iceland. In the inversion, 21 periods were used, evenly distributed from 0.01 to 100 s on a logarithmic scale. The robustness of the inversion was tested by using three different initial models: A model compiled from a joint 1D inversion of TEM and MT soundings, a homogeneous earth of resistivity 100 Ωm and a homogeneous earth of resistivity 10 Ωm. The final RMS was around 1.5 for all three models. The resulting models were elevation corrected and are presented here as smoothed resistivity maps at different elevations and as resistivity cross sections.

It is striking how the results of the 1D inversion and results of the 3D inversion based on the three initial models are similar. As one would expect, the 1D inversion reproduces the main resistivity structures while the 3D inversion shows considerably more details. The subsurface resistivity structure in Krýsuvík has the same main features as other high temperature areas in Iceland and in general where the host rocks are basaltic. Above a shallow conductive cap, a high resistivity zone is seen, reflecting unaltered rock. The conductive cap reflects smectite-zeolites hydrothermal mineral alteration. Below the low-resistivity cap, a resistive core is found, reflecting chlorite-epidote alteration. If the alteration mineralogy and the rock temperature are in equilibrium, resistivity reveals the rock temperature as well. Good correlation is seen in the Krýsuvík field between subsurface resistivity structure and hydrothermal alteration as revealed in cuttings from boreholes. Parts of the field have cooled down and, therefore, the resistivity structure indicates alteration mineralogy but not necessarily present rock temperature. The geothermal up-flow zones are most likely where the hydrothermal alteration and the resistive core reach highest elevation.

The inversion shows a relatively deep seated conductive body below the central part of the high temperature area. This body coincides horizontally approximately with an inflation source at an estimated depth of 4–5 km suggested by GPS recordings and InSAR data. The deformation was accompanied by a seismic swarm. There are no signs of S-wave attenuation and therefore, it is not likely that the body is composed of partially molten material. It has been suggested that the inflation is due to emission of gas. The deep seated conductive body is probably connected to the heat source of the geothermal field.

An analysis of the electrical strike directions based on the Tipper as well as the induction arrows are in a fairly good agreement with the final resistivity model and support it.

INTRODUCTION

The Krýsuvík high temperature geothermal area is situated on the Reykjanes peninsula, the onshore continuation of the Mid-Atlantic Ridge (see Figure 1). The active obliquely rifting plate boundaries of the American and Eurasian plates along the peninsula are characterized by a zone of high seismicity and recent volcanism, forming the transition from the offshore Reykjanes Ridge in the west to the South Iceland Seismic zone in the east. The main tectonic features are a large number of NE-SW trending volcanic fissures forming crater rows and hyaloclastite ridges and normal faults forming grabens and a series of N-S oriented right-lateral strike-slip faults. The fissures and normal faults form a series of fissure swarms arranged in a right-stepping en echelon pattern. Associated with the fissure

swarms are high temperature geothermal areas, primarily where eruptive fissures and strike-slip faults intersect.

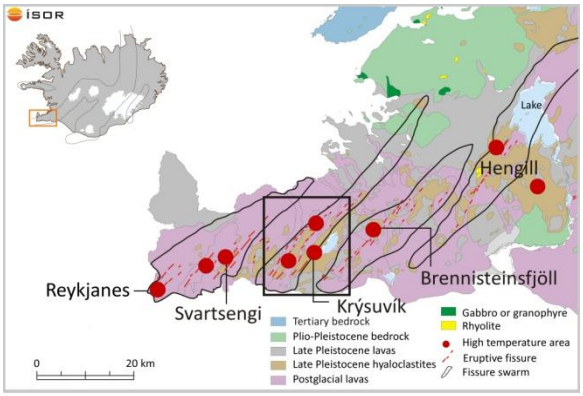

Figure 1: A geological map of the Reykjanes peninsula, based on Jóhannesson and Sæmundsson (1999). The black box indicates the Krýsuvík geothermal area and surroundings, shown in Figure 2.

Energy has been harnessed by HS Orka (formerly Hitaveita Suðurnesja) from the Reykjanes and Svartsengi geothermal fields, both located within the Reykjanes fissure swarm, for several years. Presently, in Reykjanes the power production is 100 MWe while Svartsengi provides hot water for domestic heating (150 MWth) and produces electricity (75 MWe). HS Orka has plans to exploit the Krýsuvík high temperature geothermal field in near future.

Figure 2 is an overview of Krýsuvík and its surroundings. Fumaroles, fractures and faults are according to a recent geological mapping by Sæmundsson et al., 2010. The area is characterized by a 40 km long and around 5 km wide fissure swarm and two NE-SW trending hyaloclastite ridges, Sveifluháls to the east and Núphlíðarháls-Vesturháls to the west. The ridges are 1 km wide and they rise 100-200 m above the lava fields. Reykjanes peninsula has erupted approximately once every 1000 years for the last 7000 years. The last eruption was in 1151 on a 25 km long fissure in the western part of the Krýsuvík fissure swarm. The associated high temperature areas in Krýsuvík and on the Reykjanes peninsula are different from most other high temperature areas in Iceland. No central volcano is found with a clear topographic expression, acidic rocks or a magma chamber. There are indications that Krýsuvík hosts a buried caldera and an intrusion complex in its roots (Kristján Sæmundsson, 2013, personal communication).

Iceland GeoSurvey (ÍSOR) has performed geothermal exploration in the Greater Krýsuvík area (often subdivided into Krýsuvík proper, Trölladyngja and Sandfell areas) for HS Orka for some years. A substantial part of that surveying has been a comprehensive ElectroMagnetic (EM) resistivity survey. Initially, the emphasis was on relatively shallow central-loop Transient ElectroMagnetic (TEM) survey (Eysteinsson, 1999, 2001). In recent years such shallow TEM surveys have been augmented by magnetotelluric (MT) surveys to map deeper structures (Hersir et al., 2010; Hersir et al., 2011).

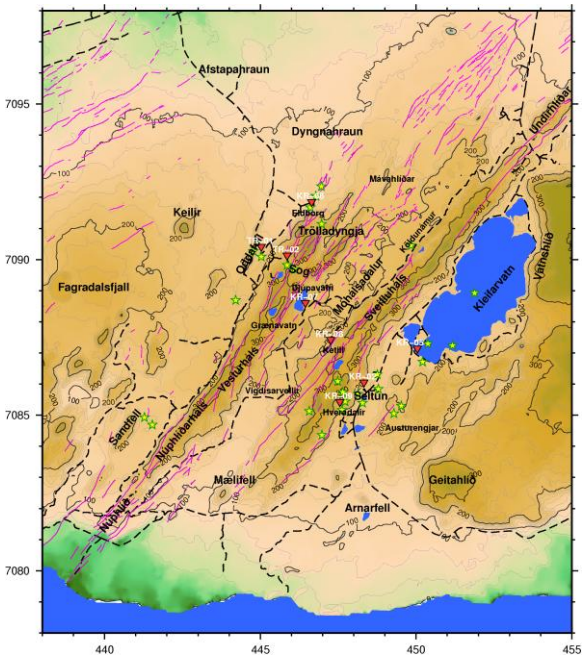

Figure 2: An overview of the survey area and the main landmarks. Wells deeper than 300 m are denoted by red filled triangles, fumaroles by green/yellow stars and fractures and faults by magenta lines. Blue color denotes the ocean and lakes.

The MT method suffers the so-called "static shift" problem. This is an inherent ambiguity in the MT data, mainly caused by local near-surface resistivity irregularities close to the sounding site (Sternberg et al., 1988; Árnason, 2008; Árnason et al., 2010). This ambiguity cannot be resolved using MT data alone. The static shift problem manifests itself in the fact that the MT apparent resistivity may contain an unknown multiplicative constant. This may lead to very wrong and misleading interpretation of the data if the static shift problem is not properly dealt with. The TEM does, on the other hand, not suffer this problem and joint inversion of TEM and MT soundings at the same location (within about 200 m) can be used to determine and correct for the static shift of the MT. Applying TEM and MT together has, therefore, by now become an industry standard. Furthermore recent developments in software and

computer technology (parallel computing on computer clusters) have made 3D inversion of MT data practical. A full 3D inversion of large MT data sets with 100–200 soundings can now be performed (e.g. Árnason et al., 2010) resulting in much more reliable and detailed results than previously attainable.

Joint 1D inversion of TEM and MT soundings from the Krýsuvík area has been performed (Hersir et al., 2010) and a provisional 2D and 3D inversion of the data was made in an MSc project at the University of Iceland (Lemma, 2010). Here a 3D inversion of static shift corrected MT data from the area is described and compared to the 1D inversion. In order to study the robustness of the results, the 3D inversion was done using three different initial models and the results are compared to the results of the joint 1D inversion. The results have been published in an internal ISOR report to the client (HS Orka) (Hersir et al., 2011).

DATA ACQUISITION

In the MT method, the natural fluctuations of the earth's magnetic field are used as signal source. Those fluctuations induce currents in the ground which are measured on the surface (E_x and E_y). The magnetic field is measured in three orthogonal directions (H_x, H_y and H_z). It is customary to have the x-direction to the magnetic north and that was done in Krýsuvík. For a homogeneous or layered earth the electrical field is induced by (coherent with) its orthogonal source magnetic field (i.e. E_x correlates with H_y, and E_y with H_x). For more complicated resistivity structures these relations become more complex. The magnetic field was measured with induction coils and the electrical field by a pair of led-chlorite filled electrodes. The electrode dipole length was in most cases 50 m.

The MT instruments used are from Phoenix Geophysics in Canada (2009), MTU type, and can measure the MT signals in the frequency range from about 400 Hz to 0.0000129 Hz. One station recorded continuously at a fixed location some 20 km north of the survey area and was used for remote reference data processing. In each sounding the MT units were deployed for recording and picked up the following day, giving about 20 hours of continuous time series. The short-period MT data (high frequency) mainly reflect the shallow structures due to their short depth of penetration, whereas the long period data mainly reflect the deeper structures. The MT method has the greatest exploration depth of all resistivity methods, some tens or hundreds of kilometres, depending on the recorded periods, and is practically the only method for studying deep resistivity structures. In this survey, the exploration depth of the MT soundings is around 30 km, but varied considerably depending on resistivity and in particular on data quality. The location of the 102 MT soundings used in the 3D inversion is shown in Figure 3.

DATA PROCESSING

The measured MT time series are Fourier transformed into the frequency domain and the "best" solution that describes the relation between the electrical and magnetic field is found by assuming the following equation:

$$\begin{bmatrix} E_x \\ E_y \end{bmatrix} = \begin{bmatrix} Z_{xx} & Z_{xy} \\ Z_{yx} & Z_{yy} \end{bmatrix} \begin{bmatrix} H_x \\ H_y \end{bmatrix} \quad (1a)$$

Or in matrix notation:

$$\vec{\boldsymbol{E}} = \boldsymbol{Z}\vec{\boldsymbol{H}} \quad (1b)$$

Where, $\vec{\boldsymbol{E}}$ and $\vec{\boldsymbol{H}}$ are the electrical and magnetic field vectors (in the frequency domain), respectively, and $\mathbf{Z}$ is a complex impedance tensor which contains information on the subsurface resistivity structure.

The tensor elements are found by minimizing the absolute square of the difference between the left and the right hand side of equation 1a with respect to the tensor elements.

For a homogeneous and 1D earth $Z_{xy} = -Z_{yx}$ and $Z_{xx} = Z_{yy} = 0$. For a 2D earth, i.e. resistivity varies with depth and in one horizontal direction, it is possible to rotate the coordinate system such that $Z_{xx} = Z_{yy} = 0$, but $Z_{xy} \neq -Z_{yx}$. For a 3D earth all the impedance tensor elements are different.

From the impedances apparent resistivity (ρ) and phases (θ) for each frequency are calculated e.g. as:

$$\rho_{xy} = 0.2T\left|Z_{xy}\right|^2;\ \theta_{xy} = \arg\left(Z_{xy}\right) \quad (2a)$$

$$\rho_{yx} = 0.2T\left|Z_{yx}\right|^2;\ \theta_{yx} = \arg\left(Z_{yx}\right) \quad (2b)$$

Programmes from Phoenix Geophysics (2005) were used to process the time series using a robust processing method technique (see e.g. Egbert and Booker, 1986). The output was then run through a software made by ÍSOR, which calculates various MT parameters and produces the results in standard EDI file format (see SEG, 1991).

3D INVERSION

The 3D inversion was performed using the inversion programme WSINV3DMT written by Weerachai

Siripunvaraporn (Siripunvaraporn et al., 2005; Siripunvaraporn and Egbert, 2009). WSINV3DMT uses finite difference forward algorithm and utilizes a formulation of the inverse problem in the data-space rather than in the model-space. This reduces the dimensionality of the problem dramatically and makes 3D inversion of MT data attainable.

Due to non-linearity the 3D inversion is an iterative minimization process. The choice of initial model can influence the final result (further discussed in the chapter about initial and prior models). 3D inversion of MT data is a highly underdetermined problem, i.e. the number of unknown resistivity values is much bigger than the number of data values. In the present case the number of data points is 8568 (102 soundings x 21 periods x 4 real and imaginary off-diagonal tensor elements, see below) but the model has 64400 unknown resistivity values (in the 50 x 46 x 28 blocks, see below) or eight times the number of data points. The inversion, therefore, needs to be regularized by imposing constraints on the model (mathematically this means to make the model parameters interdependent in such a way that the number of the actually free parameters is reduced). This can be done by constraining the model parameters to vary smoothly, often referred to as minimum structure or Occam inversion (Constable et al., 1987). Another way of regularizing is to use reference or "prior" model and constrain the inversion model not to deviate too much from the prior model. Using a prior model offers the possibility of fixing some of the model parameters to a priori known values. The inversion code uses a combination of these regularization methods and minimizes a "penalty function", which is a weighted sum of 1) the difference between measured data and calculated response (the data misfit), 2) the roughness of the model and 3) the deviation from the prior model. Initially, the inversion process quickly adjusts the model to reduce severe misfit of the data. Later on, changes that would further reduce the data misfit are rejected because they make the model deviate too much from the prior model.

The user can adjust the smoothing criteria, but not the weight of the deviation from the prior model. This can constrict the iteration from fitting the measured data adequately, especially if a model that deviates considerably from the prior model is required. Running the inversion in steps, where the initial and prior models are updated at each step (the model that gave the best fit in the previous step), can facilitate the processes of fitting the data. In this way the limitation of the prior model is gradually relaxed until the data fit can no longer be improved.

The inversion presented here is performed for the complex off diagonal elements of the MT impedance tensor, i.e. 4 numbers (2 real and 2 imaginary parts) for all periods of all soundings simultaneously.

Data preparation

The processed MT data have the x-axis in true north. In the 3D inversion programme the processed data and the model are defined in an internal (local) coordinate system or grid. It is preferable to have one of the grid axes parallel to the dominant electric (resistivity) strike. According to the strike analysis of the MT data, the Tipper strikes indicate that the dominant electric strike is close to the geological strike of N39°E. The internal coordinate system of the model is, therefore, taken to have x-axis in N39°E and consequently the y-axis in N129°E. The MT impedance tensors were, therefore, rotated by 39° to the direction of the internal system.

The 3D inversion is performed for the MT tensor elements that normally contain static shift. By assuming that the static shift is dominantly due to distortion of the electric field, the tensor can be static shift corrected by the equation:

$$\begin{bmatrix} Z^c_{xx} & Z^c_{xy} \\ Z^c_{yx} & Z^c_{yy} \end{bmatrix} = \begin{bmatrix} C_x & 0 \\ 0 & C_y \end{bmatrix} \begin{bmatrix} Z_{xx} & Z_{xy} \\ Z_{yx} & Z_{yy} \end{bmatrix} \qquad (3a)$$

$$C_x = \sqrt{1/S_{xy}} \quad ; \quad C_y = \sqrt{1/S_{yx}} \qquad (3b)$$

Where, $\mathbf{Z}^c$ is the corrected and $\mathbf{Z}$ the uncorrected tensor, respectively. S_{xy} and S_{yx} are the shift multipliers for apparent resistivity of respectively, xy and yx polarizations (Árnason et al., 2010). After the rotation of the soundings to the internal coordinate system, a joint 1D inversion was performed of the apparent resistivity and phase for both xy and yx polarizations and the nearby TEM sounding in order to determine the static shift multipliers.

The computational intensity in the inversion is directly proportional to the number of periods to be inverted for. The processed data generally contain 78 different periods ranging from about 0.003 s to 2940 s, with 13 periods per decade. To reduce the computational cost, the static shift corrected tensor was re-sampled at 21 periods equally spaced on log scale, with five values per decade, from 0.01 to 100 s. This choice of periods is a "trade off" between computational cost on one hand and resolution and depth penetration on the other. For physical consistency, the MT tensor must be a smooth function of the logarithm of the period (Weidelt, 1972). Inverting for five periods per decade is considered to give enough resolution. The period

range and the resistivity determine the depth range of exploration. The shorter the period and lower the resistivity, the shallower resistivity structures can be resolved. The longer the period and the higher the resistivity, the deeper structures can be resolved. Based on the resistivity structure in the Krýsuvík area, as revealed by the 1D inversion, it is estimated that the period range from 0.01 s to 100 s gives resolution from about 100–200 m depth and down to 10–15 km depth.

The model grid

The 3D model consists of resistivity cubes in a 3D grid mesh in the internal coordinate system. The origin (centre) of the internal coordinate system is approximately at the centre of the area of interest and data coverage and with x-axis positive towards N39°E and the y-axis positive towards N129°E. The mesh has 51 vertical grid planes in the x-direction (two edges and 49 internal planes perpendicular to the x-axis) and 47 in the y-direction (two edges and 45 internal planes) and 29 horizontal grid planes (surface, bottom and 27 horizontal internal planes). The grid is dense in the area of interest with grid plane spacing of 500 m in the area of the data coverage. Outside the dense area the grid spacing increases exponentially to the edges at ±137.5 km and ±136.5 km in the x- and y-directions, respectively. Figure 3 shows a horizontal slice of the central part of the model grid mesh with the location of the MT soundings and the coastal line of the Reykjanes peninsula.

The horizontal grid planes are likewise dense at shallow depth but the spacing increases exponentially with depth until bottom at 160 km. The shallowest layer thicknesses are 15, 25, 35, 50, 75, 100, 150, 200 m etc. (Figure 6).

Initial and prior models

As discussed earlier, 3D inversion of MT data is a highly underdetermined problem. The iterative inversion is started from an initial model. In order to regularize the inversion, a prior model is used to constrain the deviation of the resulting model from the prior model. Consequently the resulting model may depend on the initial and prior model.

Some components of the prior model can, in some cases be assumed to be known a priori and fixed in the inversion. In the case of the Krýsuvík area, the proximity of the sea has to be taken into account. Based on bathymetry, the resistivity of the model cells in the sea were assigned the average resistivity of seawater (0.3 Ωm) and kept constant during the inversion.

To investigate the influences of the initial model on the resulting model, inversions with three distinct initial models were done: a homogeneous half-space with resistivity 10 Ωm, a homogeneous half-space with resistivity 100 Ωm and a model compiled from joint 1D inversion of individual TEM/MT sounding pairs (Hersir et al., 2010). In all cases the same model was used as initial and prior model and the sea kept fixed through the inversion.

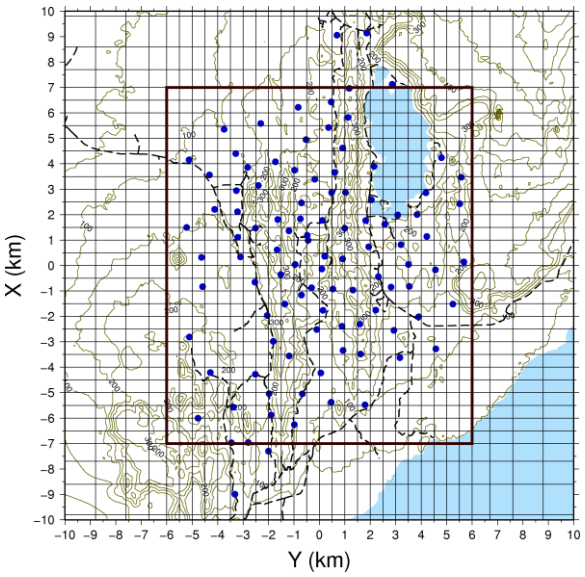

Figure 3: The central part of the model grid mesh and the coastal line of the Reykjanes peninsula. Coordinates are km in the internal (local) coordinate system. The heavy black lines mark the area of 12 x 14 km and within it the thin lines mark a 500 m x 500 m grid. The 102 MT sounding locations are shown as blue dots.

A step procedure was used during all the inversion. The inversion was allowed to run for 5 iterations at each step and restarted with the best model from previous step as initial and prior model. This stepwise inversion (and relaxation of the prior model) was continued until the data fit could not be improved any more (3-4 steps).

The inversion

The inversion programme was executed using a parallel processing version of the WSINV3DMT code using the Message Passing Interface (MPI) parallel computing environment (Siripunvaraporn and Egbert, 2009). It was executed on a 32 core computer with 132 GB memory. The inversion is a very heavy computational task and each iteration took about 5 hours and the total computing time was about 150 hours.

The data misfit is defined as the RMS (Root-Mean-Square) of the difference between the measured and calculated values, weighted by the variance of the measured values. For the 10 Ωm homogeneous half-space initial model the initial RMS misfit was 11.56 and the final misfit was 1.38. For the 100 Ωm homogeneous half-space initial model the initial RMS misfit was 40.00 and the final misfit was 1.53. For the initial model compiled from the 1D inversion the initial misfit was 6.01 and the lowest obtained misfit was 1.66. In all cases the measured data were fitted quite well. An example is given in Figure 4.

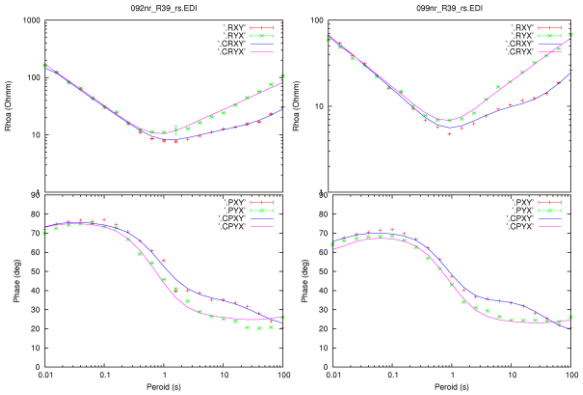

Figure 4: An example of data fit: A comparison of the (re-sampled) processed data (dots) for two soundings presented as apparent resistivity and phase and the calculated response of the final model from the inversion (unbroken lines).

PRESENTATION OF THE 3D MODEL

Visual presentation of 3D resistivity models is not straightforward. The final models are presented here in two different ways, i.e. as resistivity maps (contour plots) for different elevations (depths) and as resistivity cross sections.

Examples of the final result of the inversion based on the 100 Ωm homogeneous half space initial model are shown in Figure 5 and 6. This is a presentation of what can be called a raw model (mosaic) showing the resistivity in each cell of the model. In the smoothing and contouring process, necessary for the more conceivable plots, the center of each cell is representing it. Consequently, sections and maps are located in the middle of the cells.

WSINV3DMT assumes flat topographic surface. This seems to be a limitation, but prior to the inversion, the MT data are corrected for the static shift and this correction removes topographic effects in the data to a large extent because static shift in MT soundings is partly caused by topography (current distortion due to the topography). The resistivity models resulting from the inversion were elevation corrected, i.e. the depths below each model cell were converted to meters above or below sea level. It should be noted, when looking at the final resistivity models, that MT soundings on Lake Kleifarvatn have not been performed yet (see Figure 3).

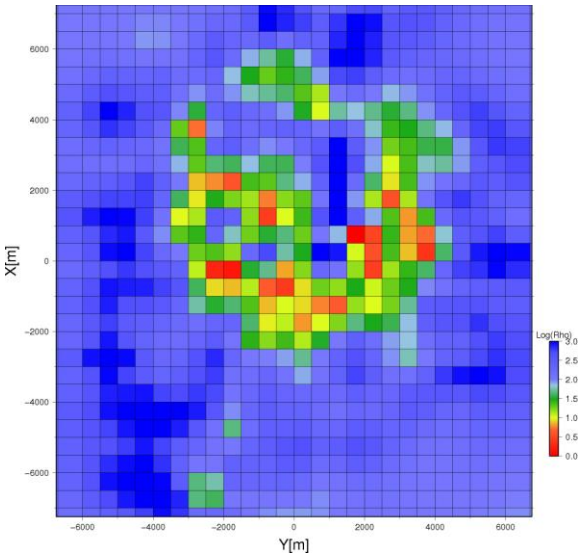

Figure 5: Raw model: resistivity at 100 m depth.

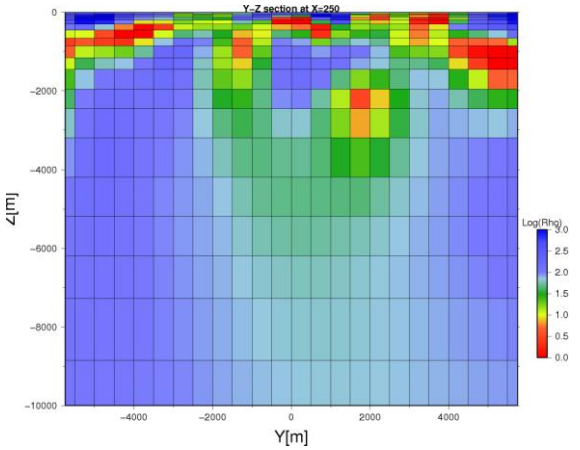

Figure 6: Raw mode: resistivity cross section.

COMPARISON OF DIFFERENT INITIAL MODELS

A representative example of the smoothed elevation corrected resistivity maps at 600 m b.s.l. are presented here showing the outcome of the inversion for all three initial models as well as the model from the 1D inversion (Figure 7 and 8).

The Figures show fracture zones inferred from the horizontal distribution of earthquakes from 1971 to 1976 and 1991 to 2001 (Magnússon and Árnason,

2002). The fracture zones are shown as broken straight black lines where their presence is not very conclusive and as unbroken black lines where the location is more convincing. The east-west lying fracture zones reflect the orientation of the plate boundaries of the American and Eurasian Plates.

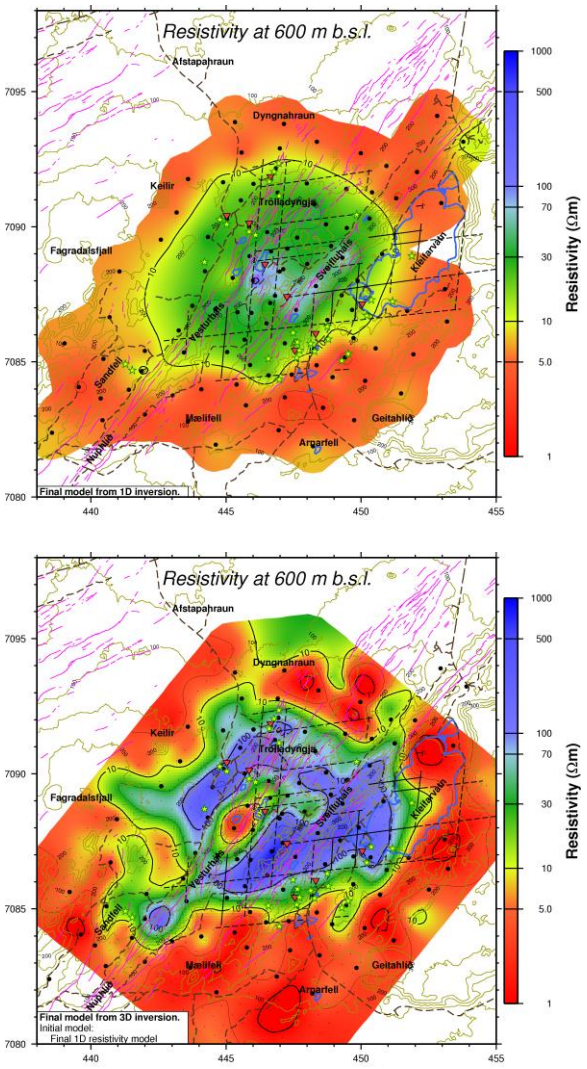

Figure 7: Resistivity models at 600 m b.s.l.: Based on 1D model (upper panel) and 3D model using the 1D model as an initial model (lower panel). Wells deeper than 300 m are denoted by red filled triangles, fumaroles by green/yellow stars and fractures and faults by magenta lines Solid and broken straight black lines show possible fracture zones, inferred from seismicity.

It is striking how the results of the 1D inversion and results of the 3D inversion based on the three initial models are similar. As one would expect, the 1D inversion reproduces the main resistivity structures while the 3D inversion shows considerably more details. It should be noted that in the case of the relatively high resistivity (100 Ωm) homogeneous half space initial model, the inversion only inserts low resistivity where needed – lending confidence in low resistivity anomalies in these models. On the other hand, for the relatively low 10 Ωm homogeneous half space initial model, the inversion only inserts high resistivity where needed – giving confidence in high resistivity anomalies in these models. The difference is clearly seen in the southern and northern parts of the models. The 3D inversion

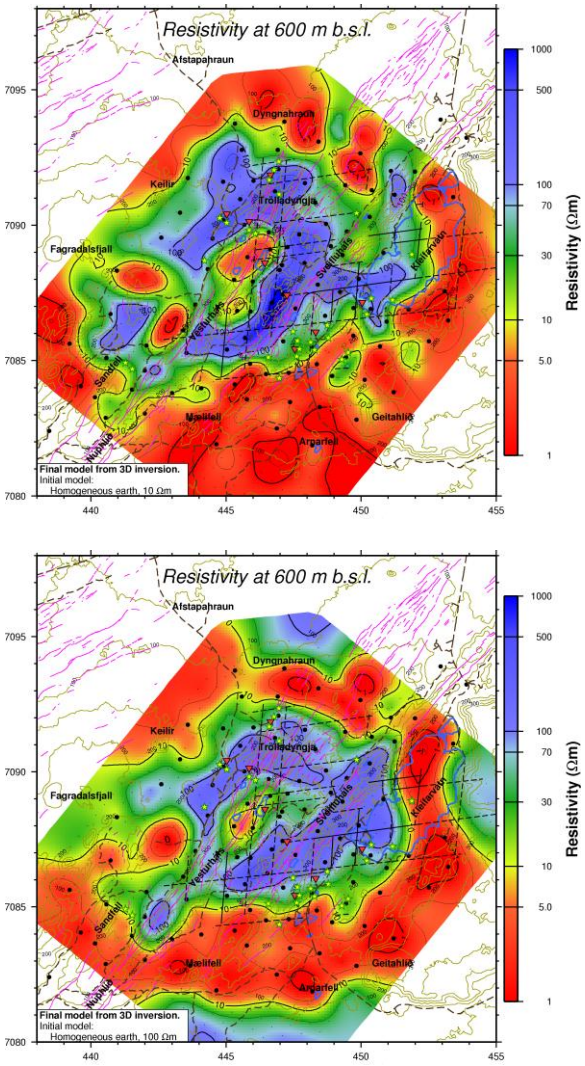

Figure 8: Resistivity models at 600 m b.s.l.: Based on 3D models, using homogeneous earth as an initial model with 10 Ωm (upper panel) and 100 Ωm (lower panel). Legend is explained in Figure 7.

model for the initial model compiled from the 1D inversion seems to be some kind of an average of the two other 3D models.

RESISTIVITY STRUCTURE OF HIGH TEMPERATURE GEOTHERMAL FIELDS

The subsurface resistivity structure of high temperature geothermal fields in Iceland as well as in other basaltic areas is broadly similar and depends mostly on hydrothermal alteration (Árnason et al., 1987; Árnason et al., 2000; Flóvenz et al., 2012), see Figure 9. Close to the surface the resistivity is high, reflecting unaltered rock – with pore fluid conduction. Below the high resistivity zone a conductive cap is found consisting of rocks with considerable amount of conductive alteration minerals, like smectite and zeolites that have high cation-exchange capacity (CEC) – with surface conduction in clay minerals. The resistivity of the cap decreases with temperature until a core of high resistivity is reached. The transition from the low-resistivity cap to the high-resistivity core coincides with a change in mineral alteration, i.e. from the high CEC smectite and zeolites to the low CEC mixed-layered clays, chlorite and epidotes – with surface and pore fluid conduction.

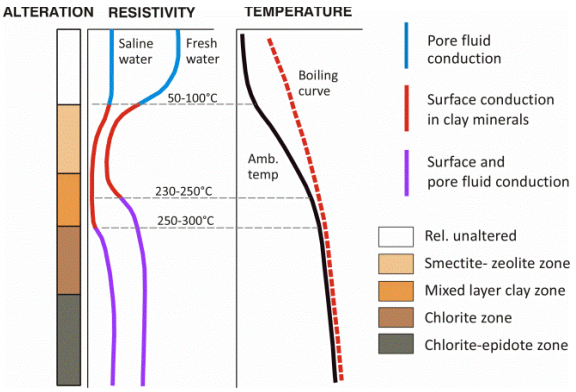

Figure 9: The general resistivity structure and alteration of the basaltic crust in Iceland summarized in Flóvenz et al. (2012); modified from Flóvenz et al. (2005).

Formation of alteration minerals depends on temperature, primary minerals and the chemical composition of the geothermal fluid. Hydrothermal alteration begins at 50-100°C and the change from smectite to chlorite type alteration assemblage occurs at temperatures close to 230°C. If the temperature that produced the alteration mineralogy prevails, the resistivity structure can be used to predict temperature. But if cooling takes place, the alteration remains and so does the resistivity structure. The resistivity structure can, therefore, in most cases be regarded as a "maximum thermometer". It has happened that alteration minerals have indicated lower temperature than measured in the wells. This has been interpreted as a young system being heated up and the alteration is lagging behind, still not in equilibrium with the temperature.

RESISTIVITY MAPS

In order to be conservative when discussing the resistivity structures in geothermal terms, especially low resistivity, the 3D model from the 100 Ωm homogeneous half space initial model is presented here. The elevations chosen are at sea level (Figure 10), 200 m b.s.l. (Figure 11), 400 m b.s.l. (Figure 12), 800 m b.s.l. (Figure 13), 1500 m b.s.l. (Figure 14) and at 5000 m b.s.l. (Figure 15). The landmarks discussed in this paragraph are shown on Figure 2.

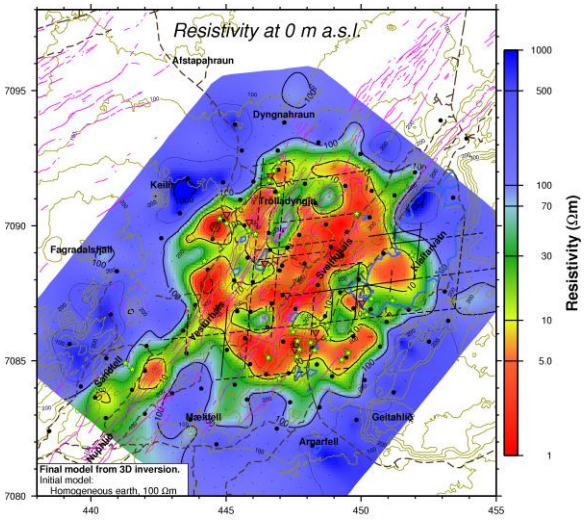

Figure 10: Resistivity at sea level. Initial model: homogeneous earth of resistivity 100 Ωm. Legend is explained in Figure 7.

At sea level (Figure 10), a circular shaped rather irregular shallow conductive cap is seen, presumably reflecting the smectite and zeolite alteration zone. Most of the fumaroles are within the zone. The circular cap is divided by the mountainous Vesturháls – Trölladyngja. The cap is absent in an area north and northeast of the fumaroles in Seltún.

At 200 m b.s.l. (Figure 11) the conductive cap reaches further to the southwest along the fissure swarm and covers the Sandfell area. A circular shaped resistive core starts to appear within the conductive cap, presumably reflecting the chlorite and epidote alteration zone. Within the core an elongated "island" of low resistivity is seen below Móhálsadalur and another one to the southwest of Djúpavatn Lake. The circular resistive core at this depth is stretching towards ENE. The resistive core reaches to the long seismic fracture zone in the south. There are no fumaroles south of the southernmost

seismic fracture zone and the zone seems to mark the southern border of the conductive cap at this depth.

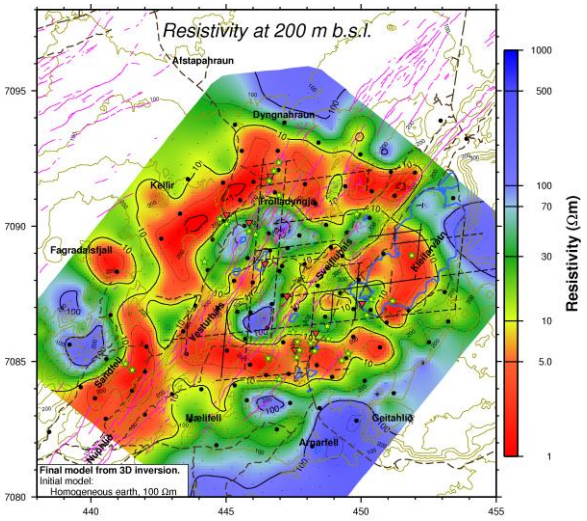

Figure 11: Resistivity at 200 m b.s.l. Initial model explained in Figure 10 and legend in Figure 7.

At 400 m b.s.l. (Figure 12) the resistive core is larger in areal extent and stretches in the direction of the fracture zones inferred from the distribution of earthquakes, shown on the Figure. The conductive "island" below Móhálsadalur has been replaced by higher resistivity. A prominent high resistivity anomaly appears along Sveifluháls. The conductive patch around Grænavatn, previously seen at 200 m b.s.l. (Figure 11), is even more striking at 400 m b.s.l. It should be kept in mind what was discussed above, namely that the inversion in this case, only inserts low resistivity where needed.

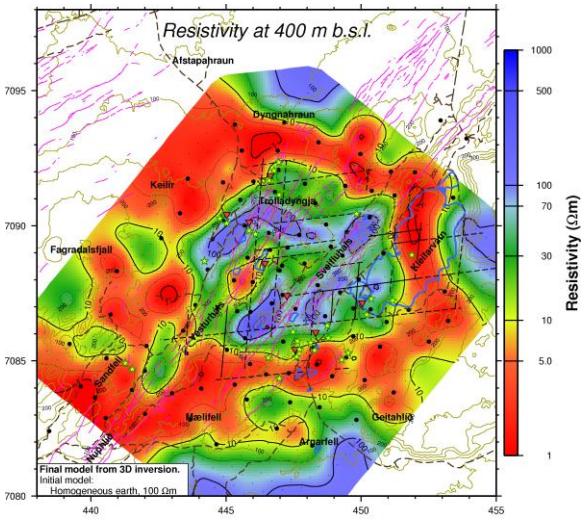

Figure 12: Resistivity at 400 m b.s.l. Initial model explained in Figure 10 and legend in Figure 7.

At 800 m b.s.l. (Figure 13) the resistive core has increased considerably in areal extent and covers the Sandfell area as well. Low resistivity is still seen below Grænavatn and to the northeast of the lake.

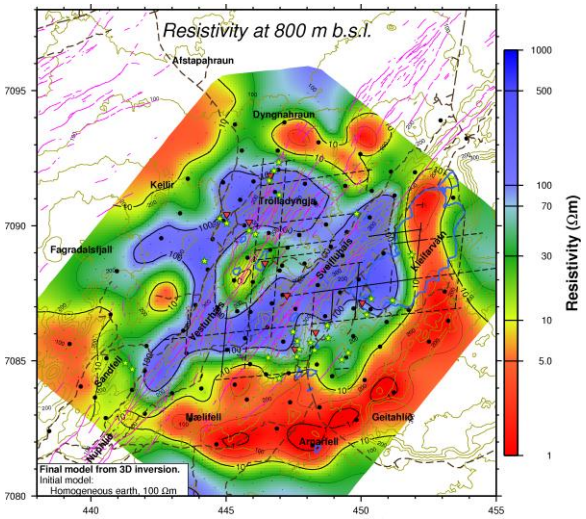

Figure 13: Resistivity at 800 m b.s.l. Initial model explained in Figure 10 and legend in Figure 7.

At 1500 m b.s.l. (Figure 14) high resistivity covers all the survey area. However, within the central part of the survey area, the main zone of faults and fractures the resistivity is relatively higher – presumably reflecting the bulk of the resistive core at that depth. The resistivity around and to the northeast of Grænavatn is still low but stretches at this depth also to the southeast. A prominent low resistivity anomaly appears just north of Seltún.

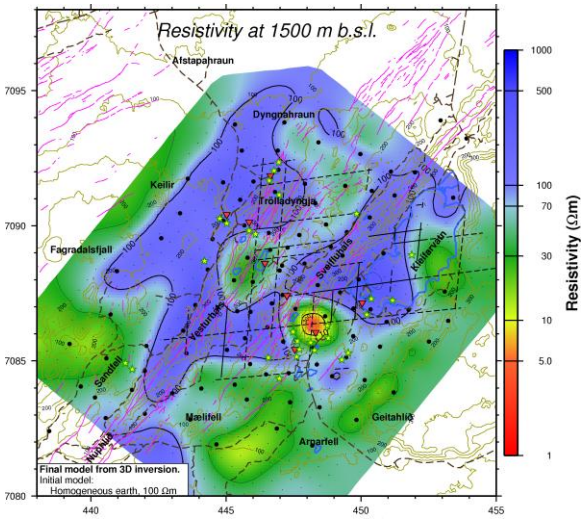

Figure 14: Resistivity at 1500 m b.s.l. Initial model explained in Figure 10 and legend in Figure 7.

At 5000 m b.s.l. (Figure 15) the detailed picture of the subsurface resistivity disappears but relatively low resistivity is still confined to the central part of the area within the main zone of faults and fractures.

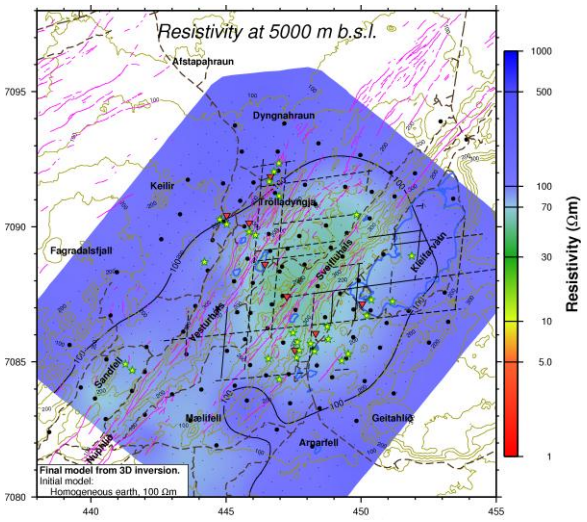

Figure 15: Resistivity at 5000 m b.s.l. Initial model explained in Figure 10 and legend in Figure 7.

According to Michalczewska et al. (2012), continuous GPS measurements suggest inflation of the Krýsuvík geothermal area in early 2009. It was confirmed by ENVISAT interferometric synthetic aperture radar data (InSAR). Inflation continued until autumn the same year when the area subsided back to pre 2009 levels. In late April 2010 another uplift episode began and continued until the end of 2011. The uplift rate exceeded 50 mm/year in 2010. Since then the area subsided slightly but has not reached the pre-inflation level. The deformation episodes were accompanied by seismic swarms. The low resistivity anomaly described above coincides horizontally approximately with an inflation source at an estimated depth of 4–5 km suggested by the deformation recordings (Michalczewska et al., 2011).

The 3D inversion of the MT data demands a relatively deep seated conductive body below Móhálsadalur somewhere between Grænavatn and Seltún, but its exact shape and location looks different depending on which initial model is used.

RESISTIVITY CROSS SECTIONS

Smoothed elevation corrected resistivity cross-sections from the 100 Ωm homogeneous half space initial model are presented in Figure 17 and 18. The sections are not along the model grid axes but across the existing wells (see Figure 16). The cross-sections also show the hydrothermal mineral alteration as revealed in cuttings from boreholes (see Hersir et al. (2010) and references therein).

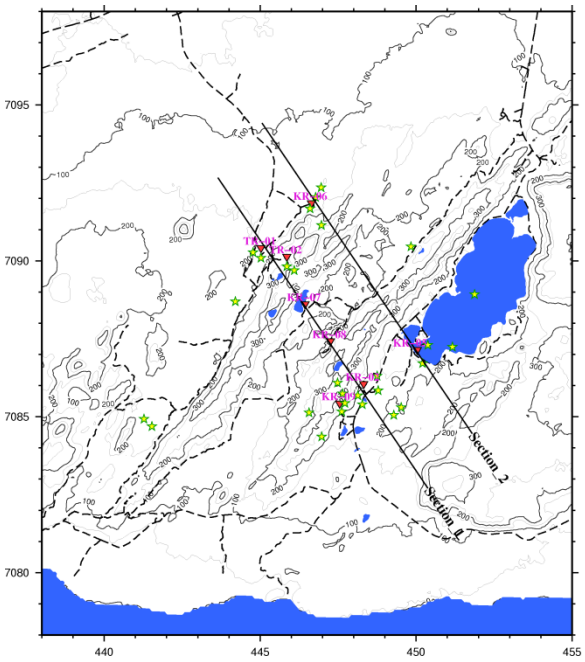

Figure 16: Location of the resistivity cross sections. Wells deeper than 300 m are denoted by red filled triangles and fumaroles by green/yellow stars.

Section 1 (Figure 17), which runs from Dyngjuhraun in the northwest through the fumaroles in Sog, across Móhálsadalur and Sveifluháls, through the fumaroles in Seltún and further to the southeast, shows the anomalously low resistivity - the conductive cap - doming up. The cap reaches highest elevation below the fumaroles in Sog (around wells TR-01 and TR-02) and Seltún (around well KR-02). Below the conductive cap, high resistivity is observed - the resistive core. Above the conductive cap, high resistivity zone is found - unaltered rock.

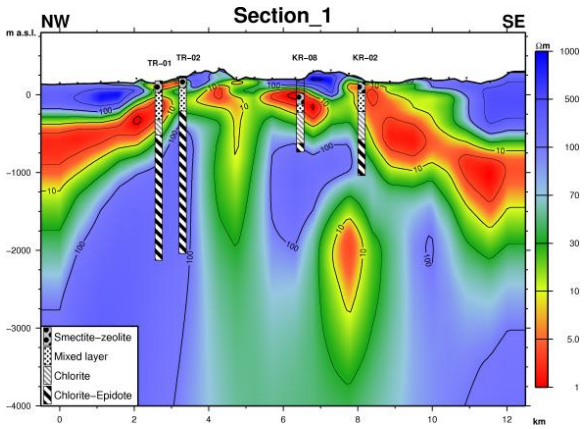

Figure 17: Resistivity cross section 1 and alteration in boreholes. Its location is shown in Figure 16.

Similar features are seen in section 2 (Figure 18). There the cap reaches highest elevation below the fumaroles close to Trölladyngja (around well KR-06) and Lake Kleifarvatn (around well KR-05).

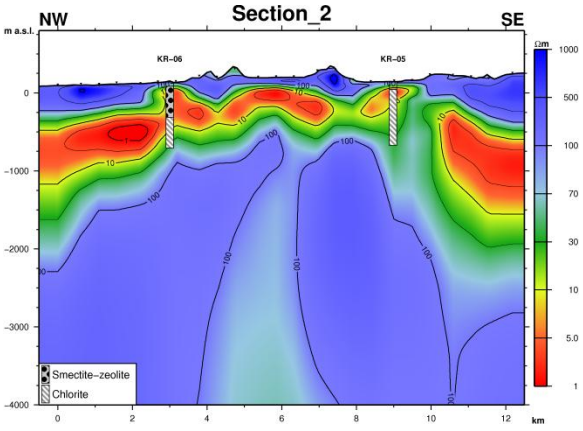

Figure 18: Resistivity cross section 2 and alteration in boreholes. Its location is shown in Figure 16.

Both of the resistivity cross sections show good correlation between the conductive cap and the smectite-zeolites alteration zone on one hand and the resistive core and the chlorite-epidote alteration zone on the other (see Figure 9).

For section 1: Rock temperature in well KR-02 and KR-08 did not reach 200°C. Their maximum temperature was 197°C at 350 m depth in well KR-02 and 190°C at 400 m depth in well KR-08, respectively. This part of the geothermal field, therefore, seems to have cooled down since the alteration took place. In well TR-02 the rock temperature is 100°C at 120 m depth, 200°C at 1200 m depth and 250°C at a depth of 1300 m. The dominant alteration is chlorite-epidote already from a depth of 500 m, clearly indicating cooling. Below 1200 m the rock temperature is higher than the alteration temperature, i.e. alteration is lagging behind. On the other hand rock temperature in well TR-01 is 100°C close to the surface and 250°C at 500 m depth. Chlorite is the main alteration mineral from a depth of 500 m – equilibrium between alteration and rock temperature. At greater depth alteration and rock temperature suggest cooling.

For section 2: In well KR-05 the highest temperature was only 181°C at a depth of 200 m – indicating cooling. In well KR-06 the rock temperature is 100°C at depth of 50–100 m, 230°C at a depth of 400 m and reaches a maximum of 262°C at 500 m depth. Chlorite is the dominant alteration from a depth of 500 m – close to equilibrium between alteration and rock temperature. However, from a depth of 650 m the temperature is almost the same, 218°C - indicating cooling at that depth.

For references on rock temperatures in wells in Krýsuvík, the reader is referred to Hersir et al. (2010) and references therein.

The conductive body discussed previously is clearly delineated in resistivity cross section 1 (Figure 17). The volume of the body having resistivity less than 10 Ωm could be around 1 km^3. Its horizontal location coincides approximately with maxima of uplift seen by GPS measurements and the deformation accompanied by a seismic swarm. There are no signs of S-wave attenuation (Kristján Ágústsson, 2013, personal communication). Therefore, it is not likely that the body is composed of partially molten material. It has been proposed that the inflation is due to emission of gas.

STRIKE ANALYSIS

Electrical strike analysis indicates the directions of lateral resistivity contrasts. These can be faults and fractures, not necessarily seen on the surface. Analysis of the strike can be an addition to the investigation on the subsurface structure and a confirmation of the resistivity model.

As discussed earlier the elements of the MT impedance tensor do, in addition to the resistivity structures below and around the site, depend on the orientation of the x- and y-axis of the field layout. For a 2D earth, the resistivity varies with depth and in one horizontal direction. The horizontal direction perpendicular to that direction is called the geo-electrical strike. The angle, Φ it makes with geographical north is called Swift-angle or Zstrike. It is possible to rotate the coordinate system by mathematical means and recalculate the elements of the impedance tensor for any desired direction. This equals that the fields (**E** and **H**) had been measured in these rotated directions. If the earth is 2D and the coordinate system of the field layout has one axis parallel to the geo-electrical strike direction, then: $Z_{xx} = Z_{yy} = 0$, but $Z_{xy} \neq -Z_{yx}$. The geo-electrical strike, Zstrike, can be determined by minimizing: $|Z_{xx}|^2 + |Z_{yy}|^2$ with respect to Φ - the rotation of the coordinate system. There is, however, a 90° ambiguity in the strike angle determined in this way and no way of distinguishing between Φ and $\Phi + 90°$, from the tensor alone.

The depth of investigation increases with the period and Zstrike depends on the period because the dominant geo-electrical strike can be different at different depths. Another parameter that is often used

for directional analysis is the so-called Tipper, $\boldsymbol{T}$, which relates the vertical component of the magnetic field to its horizontal components:

$$\boldsymbol{H}_z = T_x \boldsymbol{H}_x + T_y \boldsymbol{H}_y \qquad (4)$$

T_x and T_y are the x- and y-component of the Tipper, respectively. For 1D earth the Tipper is zero, $T_x = T_y = 0$. For a 2D earth, the coordinate system can be rotated so that the x-axis is in the strike direction, the so-called Tstrike, i.e. $T_x = 0$, but $T_y \neq 0$. This is done by minimizing $|T_x|$. By proper definition, the Tstrike does not suffer the 90° ambiguity of the Zstrike.

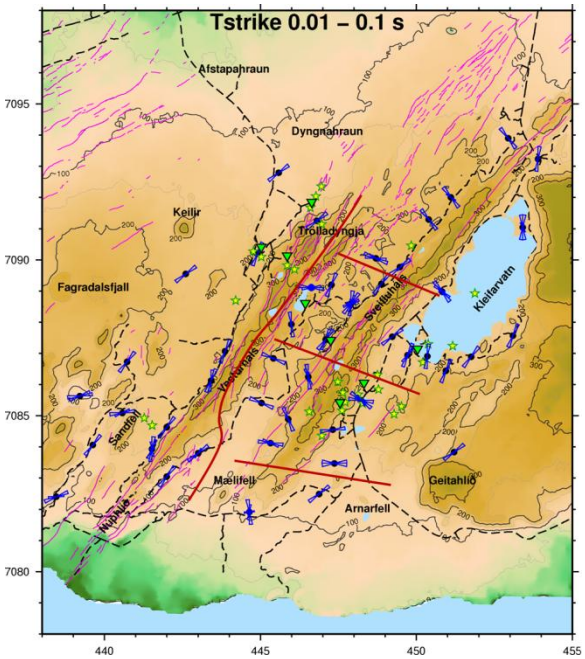

Figure 19: Rose diagram of the Tipper strike for the period, 0.01–0.1 s. Thick dark red lines indicate zones of different dominant strike directions. Wells deeper than 300 m are denoted by green filled triangles, fumaroles by green/yellow stars and fractures and faults by magenta lines.

The rose diagram on Figure 19 shows the Tstrike for period, 0.01–0.1 s, corresponding to a depth of several hundred meters. Firstly, the diagram broadly reflects and partly encircles the main resistivity structure as revealed in Figures 10 to 13, lending confidence to the final resistivity model. Thick dark red lines are drawn on the Figure indicating zones of different dominant Tstrike directions. However, it must be kept in mind that these lines are by no means unambiguous, simply an indication. To the west of Vesturháls and Trölladyngja, the Tstrike is along the dominant geological strike and the youngest eruption fissures in Krýsuvík and parallel to the NW lying resistivity boundaries. To the east of Vesturháls, the Krýsuvík area can be divided into four zones, two of them showing dominant electrical strike direction perpendicular to the geological strike. In the northernmost and the two southernmost zones, the Tstrike is parallel to the main resistivity contrasts, which is in fairly good agreement with the final resistivity model. The zone covering the southern part of Lake Kleifarvatn is within the low resistivity anomaly. There, the Tstrike is more irregular which is consistent with the small sized induction arrows in that area (Figure 20). The rose diagrams for periods higher than a few seconds are totally dominated by the conductive sea, i.e. the Tstrike is parallel to the coast (Hersir et al., 2011), and do not add anything to the resistivity study of the area.

The Tipper, ***T,*** is a complex (two component) vector and can be represented as two real vectors, or induction arrows, the real part and the imaginary part. According to the sign convention used here, the real arrows point away from a zone of low resistivity at sufficiently low frequencies and towards a zone of higher resistivity (Berdichevsky and Dmitriev, 2002).

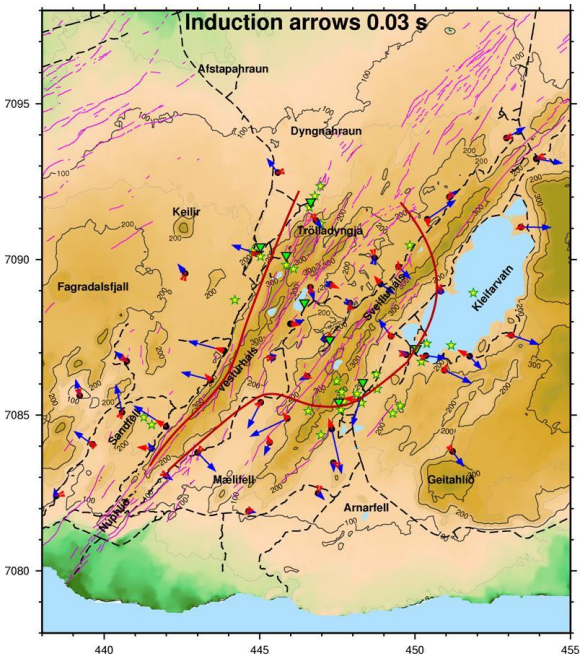

Figure 20: Induction arrows for the period 0.03 s. Blue arrows denote the real part and red arrows the imaginary part. Thick dark red lines denote presumed boundaries of a good conductor according to the induction arrows. Legend is explained in Figure 19.

The induction arrows are shown for the period 0.03 s in Figure 20, corresponding to a depth of several hundred meters. Thick dark red lines have been

drawn on the Figure indicating the approximate location of the main conductor. In general the induction arrows point away from the conductor and reflect quite well the main resistivity structure as revealed in Figures 10 to 13, again lending confidence to the final resistivity model. For periods higher than a few seconds, the real part of the induction arrows point away from the coast, being totally dominated by the conductive sea (Hersir et al., 2011).

DISCUSSION AND CONCLUSIONS

A 3D inversion was performed for static shift corrected off diagonal impedance tensor elements of 102 MT soundings in the Greater Krýsuvík area, SW Iceland. The robustness of the final inversion model was tested by using three different initial models.

The results of the 1D inversion and results of the 3D inversion with the three initial models are strikingly similar. As one would expect, the 1D inversion reproduces the main resistivity structures while the 3D inversion shows considerably more details. In the case of the relatively high resistivity (100 Ωm) homogeneous half space initial model, the inversion only inserts low resistivity where needed – lending confidence in low resistivity anomalies in these models. Here, the resistivity maps and cross sections are based on that initial model.

The resistivity model in Krýsuvík reflects different hydrothermal alteration minerals and there is good agreement between the subsurface resistivity structure and the alteration minerals as revealed in cuttings from boreholes. High resistivity zone is found close to the surface corresponding to unaltered rock, below it is a conductive cap with smectite-zeolites alteration minerals, followed by the resistive core with chlorite-epidote alteration minerals. In most of the area where temperature logs exist, cooling has taken place except in well TR-01 and party in KR-06, both in the northwestern part close to the youngest eruptive fissure.

The resistivity structure shows a circular anomaly, which stretches to the southwest along the fissure swarm as well as towards ENE and correlates with the fracture zones delineated by earthquakes.

The 3D inversion of the MT data demands a relatively deep seated conductive body below Móhálsadalur somewhere between Grænavatn and Seltún, but its exact shape and location looks different depending on which initial model is used. Based on the homogeneous earth of resistivity 100 Ωm as the initial model, a low resistivity body is revealed at about 2 km depth just north of Seltún with an estimated volume of around 1 km^3. Horizontal location of this anomaly coincides with an inflation source at an estimated depth of 4–5 km suggested by GPS recordings and confirmed by InSAR data. The crustal movement seems to be accompanied by a seismic swarm. No S-wave attenuation is observed, indicative of melt. It has, therefore, been proposed that the inflation is due to emission of gas.

Electrical strike directions based on the Tipper and induction arrows are consistent with the resistivity model and support it.

ACKNOWLEDGMENTS

The authors acknowledge HS Orka for allowing the use of the data. Kristján Ágústsson geophysicist at ÍSOR read carefully the whole text and gave valuable comments and suggestions. Andemariam Teklesenbet Beyene geophysicist from Eritrea presently working at ISOR assisted in various ways. The authors acknowledge them for their contribution.

REFERENCES

Árnason, K., Flóvenz, Ó., Georgsson, L.S., and Hersir, G.P. (1987), "Resistivity structure of high temperature geothermal systems in Iceland," *International Union of Geodesy and Geophysics (IUGG) XIX General Assembly*, Vancouver, Canada, Abstracts V, 477.

Árnason, K., Karlsdóttir, R., Eysteinsson, H., Flóvenz, Ó.G. and Gudlaugsson, S.Th. (2000), "The resistivity structure of high-temperature geothermal systems in Iceland," *Proceedings of the World Geothermal Congress 2000, Kyushu-Tohoku, Japan*, 923–928.

Árnason, K. (2008), "*The Magnetotelluric static shift problem,*" Iceland GeoSurvey, report, ÍSOR-08088, 16 pp.

Árnason, K., Eysteinsson, H. and Hersir, G.P. (2010), "Joint 1D inversion of TEM and MT data and 3D inversion of MT data in the Hengill area, SW Iceland," *Geothermics*, **39**, 13–34.

Constable, C. S., Parker, R. L. and Constable, C. G. (1987), "Occam's inversion: a practical algorithm for generating smooth models from electromagnetic sounding data," *Geophysics,* **52**, 289–300.

Berdichevsky, M.N. and Dmitriev, V.I. (2002), "Magnetotellurics in the context of the theory of ill-posed problems," *Society of Exploration Geophysicists*, 215 pp.

Egbert, G.D. and Booker, J.R. (1986), "Robust estimation of geomagnetic transfer functions," *Geophys. J. R. Astr. Soc.* **87**, 173–194.

Eysteinsson, H. (1999), "*Resistivity measurements around Sandfell, Reykjanes Peninsula,"* NEA Report OS-99002, 71 pp. (in Icelandic).

Eysteinsson, H. (2001), "*Resistivity measurements around Trölladyngja and Núpshlíðarháls, Reykjanes Peninsula,"* NEA Report OS-2001/038, 110 pp. (in Icelandic).

Flóvenz, Ó.G., Hersir, G.P., Saemundsson, K., Ármannsson, H. and Fridriksson, Th. (2012), "Geothermal Energy Exploration Techniques." *In: Sayigh, A., (ed.) Comprehensive renewable energy, Volume 7. Elsevier, Oxford, 51-95.*

Flóvenz, Ó.G., Spangenberg, E., Kulenkampff, J., Árnason, K., Karlsdóttir, R. and Huenges, E. (2005), "The role of electrical conduction in geothermal exploration," *Proceedings World Geothermal Congress 2005, Antalya, Turkey, CD, 9 pp.*

Hersir, G. P., Vilhjálmsson, A. M., Rosenkjær, G. K., Eysteinsson, H. and Karlsdóttir, R. (2010), "*The Krýsuvík geothermal field. Resistivity soundings 2007 and 2008,"* Iceland GeoSurvey, report, ÍSOR-2010/025, 263 pp. (in Icelandic).

Hersir, G. P., Árnason, K., and Vilhjálmsson, A. M. (2011), *"3D inversion of MT data from Krýsuvík, SW Iceland*," Iceland GeoSurvey, report, ÍSOR-2011/072, 165 pp.

Jóhannesson, H. and Sæmundsson, K. (1999*), "Geological map of Iceland 1:1.000.000*," Icelandic Institute of Natural History.

Lemma, Y. D. (2010), *"Multidimensional inversion of MT data from Krýsuvík High Temperature Geothermal Field, SW-Iceland, and study of how 1D and 2D inversion can reproduce a given 2D/3D resistivity structure using synthetic data*," Master's thesis, Faculty of Earth Sciences, University of Iceland, 119 pp.

Magnússon, I.Þ. and Árnason, K. (2002), "*Earthquakes and fractures around Trölladyngja and Krýsuvík. Comparison with specific resistivity,"* Orkustofnun, report, OS-2002/048, 24 pp. (in Icelandic).

Michalczewska, K., Hreinsdóttir, S., Auriac, A., Ágústsdóttir, T., Árnadóttir, T., Geirsson, H., Hooper, A., Feigl, K.L., Bennet, R., Einarsson, P., Sigmundsson, F., Decriem, J., Keiding, M., Steinþórsson, S. and Hensch, M. (2011), "The inflation and deflation episodes in the Krísuvík geothermal area*," Poster at the Institute of Earth Sciences, University of Iceland.*

Michalczewska, K., Hreinsdóttir, S., Árnadóttir, Th., Hjaltadóttir, S., Ágústsdóttir, Th., Gudmundsson, M.T., Geirsson, H., Sigmundsson, F. and Gudmundsson, G.B. (2012), "The inflation and deflation episodes in the Krísuvík volcanic system," *Abstract ID: V33A-2843, AGU Fall Meeting, December 2012.*

Phoenix Geophysics (2005), "*Data Processing User Guide,"* Phoenix Geophysics, 201 pp.

Phoenix Geophysics (2009), "*V5 System 2000 MTU/MTU-A User Guide,"* Phoenix Geophysics. 178 pp.

SEG (1991), "*MT/EMAP data interchange standard*," Society of Exploration Geophysicists, 112 pp.

Siripunvaraporn, W., Egbert, G., Lenbury, Y. and Uyeshima, M. (2005), "Three-dimensional magnetotelluric inversion: data-space method," *Phys. Earth Planet. Int.*, **150**, 3–14.

Siripunvaraporn, W. and Egbert, G. (2009), "WSINV3DMT: Vertical magnetic field transfer function inversion and parallel implementation," *Phys. Earth Planet. Int.*, **173**, 317–329.

Sternberg, B. K., Washburne, J. C. and Pellerin, L. (1988), "Correction for the static shift in magnetotellurics using transient electromagnetic soundings," *Geophysics*, **53**, 1459–1468.

Sæmundsson, K., Jóhannesson, H., Hjartarson, Á. and Kristinsson, S. G. (2010), "*Geological map of Southwest Iceland, 1:100.000,"* Iceland GeoSurvey.

Weidelt, P. (1972), "The inverse problem of geomagnetic induction," *J. Geophys.*, **38**, 257–289.